# Wafer-Scale Method of Controlling Impurity-Induced Disordering for Optical Mode Engineering in High-Performance VCSELs

Patrick Su<sup>®</sup>, Member, IEEE, Fu-Chen Hsiao, Thomas O'Brien, Jr.<sup>®</sup>, and John M. Dallesasse, Fellow, IEEE

Abstract-Impurity-induced disordering (IID) provides a wafer-scale method of enhancing the performance of vertical-cavity surface-emitting lasers (VCSELs) for applications requiring higher output power in a specific optical mode. IID has been demonstrated to achieve higher optical power, faster modulation, and single-mode operation in oxide-confined VCSELs. Through the formation of an IID aperture, spatial control of mirror reflectivity can be selectively used to increase the threshold modal gain of only selected optical modes. However, these IID apertures have been limited by the lack of a method to control the shape of the diffusion front. For maximum laser mirror loss, IID apertures employed for mode-control require deep disordering. Consequently, significant lateral diffusion can be present that undesirably increases the lasing threshold for the fundamental mode. A manufacturable method is presented for controlling the shape of the IID aperture diffusion front by tailoring the strain of the diffusion mask. Experimental analysis to determine an optimal IID aperture size for single-mode high-power operation is next discussed. Numerical analysis of the mirror losses induced and consequent reduction in supported higher order modes as a result of the IID aperture is then presented.

Index Terms—Vertical-cavity surface-emitting laser, single-fundamental-mode, impurity-induced disordering, wafer-scale manufacturing, compound semiconductors.

## I. INTRODUCTION

ERTICAL—CAVITY Surface-Emitting Lasers (VCSELs) have become one of the most ubiquitous lasers in modern consumer markets. Their small footprint, circular-beam profile, on-wafer probing capability, and high reliability are especially advantageous for volume manufacturing and packaging, leading to applications in data communications, position sensors (optical "mice"), cellular telephone facial recognition and 3-D imaging, and sensors for autonomous vehicles [1].

VCSELs are inherently single-longitudinal-mode lasers due to their extremely short optical cavity length. The transverse

Manuscript received July 2, 2018; revised August 14, 2018; accepted August 14, 2018. Date of publication August 17, 2018; date of current version October 29, 2018. This work was supported in part by E2CDA-NRI, a funded center of NRI, a Semiconductor Research Corporation program sponsored by NERC and NIST under Grant NERC 2016-NE-2697-A, and in part by the National Science Foundation under Grant ECCS 16-40196 and Grant NSF ACI 16-59, and in part by the II-VI Foundation. (Corresponding author: Patrick Su.)

The authors are with the Department of Electrical and Computer Engineering, University of Illinois at Urbana-Champaign, Urbana, IL 61801 USA (e-mail: psu8@illinois.edu; fhsiao3@illinois.edu; tobrien3@illinois.edu; jdallesa@illinois.edu).

Digital Object Identifier 10.1109/TSM.2018.2866065

dimension however, which is defined by the diameter of the device, is typically many multiples of the wavelength in the material. As a consequence, conventional VCSELs suffer from multi-mode emission that limits their ability to form coherent beams, especially over long distances. In emerging applications such as 3D facial recognition and light detection and ranging (LIDAR), both single-fundamental-mode and high-power (milliwatt) emission is necessary to achieve satisfactory performance.

Early demonstrations of vertically-emitting semiconductor lasers were achieved with metal mirrors by Melngailis in 1965 [2] and by Iga in 1979 [3]. However, the laser threshold current, resulting from losses in the metallic reflectors in addition to poor overlap of the electric field with the gain, was too high for practical applications. Even with the innovating adoption of distributed Bragg reflectors (DBRs) [4] as optical mirrors in VCSELs, it was the discovery of native oxide growth in AlGaAs by Dallesasse et al. [5], [6] and its application to form oxide apertures by Huffaker et al. [7] that led to the low-threshold, energy-efficient, and reliable operation of modern VCSELs. The use of an oxide aperture not only provides enhanced electrical and optical confinement, but also reduces the active device diameter thereby suppressing higher order modes. In order to enable VCSELs for emerging applications that require single-mode emission, several methods of mode-control have been developed. The most direct approach to achieving single-mode operation is to reduce the oxide-aperture size until the device is no longer capable of supporting higher order modes. While single-mode operation has been reported using this method [8], it concurrently led to increased self-heating, lower output powers and shorter lifetimes [9]. More intricate methods of mode-control have been developed that exploit the spatial discrimination between the fundamental mode and higher order modes. In a VCSEL structure, the electric-field of the fundamental mode is concentrated in the center while the higher order modes lie further radially away. By creating increased mirror or index guiding losses near the outer edge of the VCSEL, particularly in regions strongly overlapping the higher order modes, it has been reported that single-fundamental-mode operation can be achieved. Such methods that have demonstrated with varying degrees of success include the surface-relief method [9], [10], photonic crystal VCSELs [11], high-contrast gratings [12] and anti-resonant reflecting optical waveguide (ARROW) designs [13]. However, the disadvantage of

some of these methods is that they require either expensive and low-yield regrowth processes or fabrication of complex structures that limit their scalability for high-volume manufacturing.

## II. IMPURITY-INDUCED DISORDERING

Since the early development of semiconductor processing technologies, atomic diffusion has played a vital role in wafer-scale manufacturing. The capability to introduce foreign species in a controllable, non-destructive, and low-cost manner has led to the establishment of diffusion as a core process. Impurity-induced disordering (IID), initiated by the diffusion of Zn, provides the capability to enhance the performance of optoelectronic devices on a wafer-scale. Impurity-Induced Disordering was first discovered by Laidig et al. [14] with the diffusion of Zn into an AlAs-GaAs superlattice. It was found that by the diffusion of impurities through a superlattice, the discrete AlAs-GaAs layers would intermix, resulting in a homogenous indirect bandgap bulk Al<sub>x</sub>Ga<sub>1-x</sub>As material with an averaged aluminum composition [14], [15]. The value of impurity-induced disordering for VCSELs lies in the capability to affect the power-reflectivity of the mirrors. When Zn disorders the DBR of a VCSEL, both the power-reflectivity and stop band spectral width of the mirror greatly decrease [16], [17]. Furthermore, Zn diffusion increases free-hole concentration in the disordered areas thus promoting optical free-carrier absorption, increasing optical loss. Reducing mirror reflectivity and increasing optical loss creates a spatial variation in the threshold gain for lasing. Through the spatially selective diffusion of Zn into the upper DBR, significant performance enhancement with respect to mode discrimination can be achieved. Similar to the surfacerelief method, IID can be used for mode-control by decreasing the mirror-reflectivity in regions that primarily overlap higher order modes. The advantage of IID over the surfacerelief method is that IID does not degrade the topology of the VCSEL, specifically, the highly conductive cap layer. Therefore, uniform current injection and low series resistance is still maintained for disordered VCSELs. This is achieved because the diffused Zn acts as an additional p-type dopant, thereby reducing both the contact and series resistance by nearly a factor of three relative to as-grown material [16], [17]. IID employed in VCSELs has also demonstrated higher modulation speeds [18], lower energy-to-data rate ratios [19], and greater output powers [20] than conventional oxide-confined VCSELs.

Previous work has shown the capability to enable high-power single-mode operation in VCSELs by employing impurity-induced disordering [16], [17]. However, these devices have been greatly limited in their IID aperture design due to the profile of the diffusion front that determines the lateral-to-vertical dimension of the IID aperture. When deep diffusions are desired to maximize the amount of mirror loss impinged on higher order modes, the IID aperture size is limited by the lateral dimension of the diffusion front and its overlap with the fundamental mode. We have therefore developed a method based on engineering the strain induced

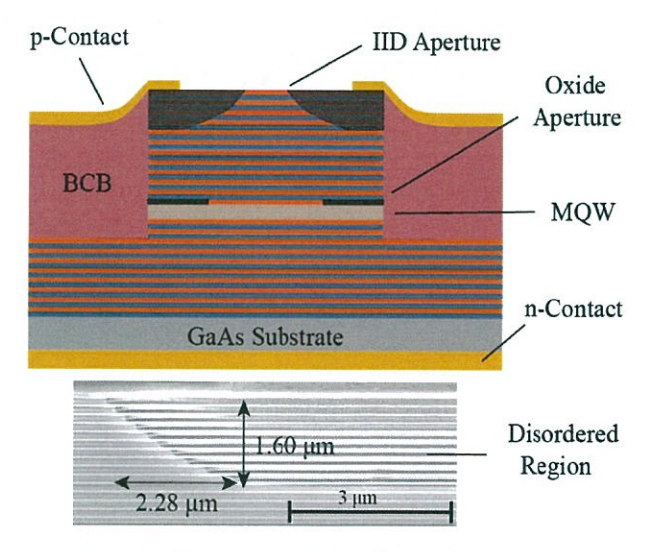
by the diffusion mask to control the diffusion front. This work demonstrates the capability of tailoring the IID aperture's diffusion front on a wafer-scale level. Modeling and numerical calculations of various IID apertures and their effects on propagating modes in oxide-confined VCSELs is also presented to analyze the optimal IID aperture size for high-power single-mode operation.

#### III. DESIGN AND FABRICATION

The epitaxial structure employed in this work consists of 37 n-type AlGaAs-based bottom DBR pairs, 3 undoped GaAs quantum wells serving as the active region located in the middle of a half-wavelength thick Al<sub>0.3</sub>Ga<sub>0.7</sub>As cavity, and 20 p-type AlGaAs-based DBR pairs which is grown on a GaAs substrate. The DBR pairs are composed of alternating Al<sub>0.15</sub>Ga<sub>0.85</sub>As and Al<sub>0.90</sub>Ga<sub>0.10</sub>As layers designed to support an emission wavelength of 850 nm. A single high-aluminum content layer is grown directly above the active region in order to allow the formation of an oxide aperture during fabrication. There is a highly conductive GaAs cap layer on top of the upper p-type DBR that enhances current spreading for improved current injection. This cap layer is etched down to 100 nm in thickness as this has been shown to reduce phaserelated mirror loss for this epitaxial structure that has been employed in our previous work [16], [17], [20].

Following the cap etch, disordering is completed in the upper DBR. In order to selectively diffuse Zn into an aperture, SiNx is deposited on the surface utilizing an STS Multiplex Plasma-Enhanced Chemical Vapor Deposition (PECVD) system with a high-frequency (13.56 MHz) plasma source. The deposited SiNx is then patterned via photolithography and RIE etching in order to form circular pillars covering the center of the VCSELs. The patterned SiNx serve as a diffusion mask, where the diameter defines the IID aperture size that is formed. In order to diffuse Zn, these masked epitaxial samples are sealed under vacuum ( $<5 \times 10^{-6}$  Torr) in a quartz ampoule along with a solid ZnAs2 source. The quartz ampoule is then loaded into a dry furnace at 600°C for 80 minutes. Other work has demonstrated the ability to diffuse Zn on a wafer-scale compatible with this process [21], [22].

Once the disordering process is completed, the SiNx diffusion mask is removed and a traditional oxide-confined VCSEL is fabricated from the disordered epitaxial samples. In order to define the VCSEL mesas, a SiNx dielectric hard mask is deposited and patterned via lithography. Utilizing an Oxford PlasmaLab System 100 Inductively Coupled Plasma-Reactive Ion Etching (ICP - RIE) system, the VCSEL mesas are defined using a composition of BCl<sub>3</sub>/H<sub>2</sub>/Ar gasses to achieve anisotropic etching and minimize sidewall roughness. The etching process is monitored by an in-situ laser interferometry apparatus to precisely halt the etching process once the high aluminum Al<sub>x</sub>Ga<sub>1-x</sub>As layer for selective oxidation has been exposed. The etched samples are then placed in a wet furnace set at 405°C that contains a continuous flow of a gaseous H<sub>2</sub>O/N<sub>2</sub> mixture in order to laterally oxidize and form oxide confinement apertures for control of optical confinement and



· Fig. 1. Cross-sectional schematic of an oxide-confined VCSEL with an IID aperture (top). An SEM image of the resulting disordered top DBR layer is also shown (bottom).

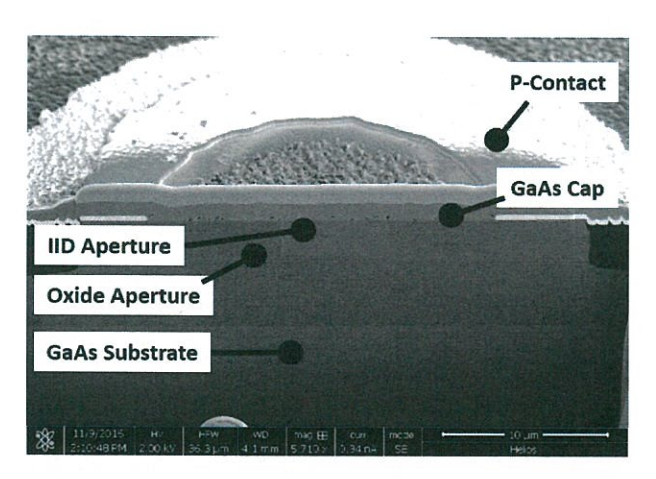


Fig. 2. FIB-SEM image providing a cross-sectional view of a fabricated IID VCSEL.

electrical current injection [7]. The devices are planarized with benzocyclobutene (BCB) and metalized with a top pelectrode layer (Ti/Pt/Au) via electron-beam evaporation. The backside GaAs substrate is thinned down using an aluminumoxide slurry and finished with a chemical mechanical polishing (CMP) process. Subsequently, an n-type (AuGe/Ni/Au) contact is deposited and alloyed at 405°C to form an ohmic backside contact. A cross-sectional schematic of an impurityinduced disordered VCSEL in addition to a scanning electron microscope (SEM) image of an IID aperture is shown in Fig. 1. In addition, a focused ion beam scanning electron microscope (FIB-SEM) image providing a cross-sectional view of a fabricated IID VCSEL is shown in Fig. 2. It should be noted that a platinum protective layer is deposited over the top surface of the device prior to ion milling. This layer is seen above the GaAs cap. Under normal operation, this layer is not present.

## IV. DEVICE CHARACTERIZATION

Reported in our previous work [16],[17],light-current-voltage (LIV) and maximum-fundamental-mode output power is recorded for various sized IID apertures. It has been found that if the IID aperture is small (<0.4 µm). then all of the propagating modes will incur mirror losses introduced by the disordering. While single-mode operation is maintained for the entire current drive of the smaller IID aperture devices, the output power is severely limited by self-heating since the large disordered region also acts as a highly concentrated doping region and contributes to free-carrier absorption. As the IID aperture size begins to increase to an optimal size ( $\sim$ 1.3  $\mu$ m), the fundamental-mode as well as a few higher order modes begin to see less influence from the disordered region. While this leads to a higher maximum-fundamental-mode output power, higher order modes begin to appear at larger injection current levels. Lastly, as the IID aperture size increases to its largest size (1.6 µm), the highest total output power is achieved, however, the emission is found to be multi-mode.

For the application of mode control in VCSELs, it is ideal that the IID aperture is as deep as possible to ensure large higher order mode mirror loss in order to guarantee single-mode operation. However, increased vertical diffusion also results in increased lateral diffusion. The degree of lateral diffusion is dependent on the initial diffusion front that is formed. It is therefore apparent that the capability to form geometrically tailored diffusion fronts can enable more application specific and intricate IID aperture designs.

## V. CONTROL OF IID APERTURE

The capability to control the IID aperture profile through engineering the strain that is induced by the diffusion mask is introduced. Utilizing an STS Multiplex PECVD system that is capable of alternating between a high-frequency (13.56 MHz) and low-frequency (680 KHz) plasma source during deposition, mixed compositions of high-frequency and low-frequency sourced SiN<sub>x</sub> diffusion masks can be deposited. During this process, the chamber pressure, gas flow, and plasma power are fixed to eliminate any process variable other than the plasma source frequency. The chamber pressure is 650 mT, SiH<sub>4</sub> flow is 40 sccm, NH<sub>3</sub> flow is 55 sccm, and N<sub>2</sub> flow is 1960 sccm. Both power supplies are set to 20 W, and the deposition thickness is maintained at 50 nm. By using a GaAs witness wafer, both high-frequency and low-frequency SiNx films are deposited and their film stress are measuremed using a FSM 500TC thin film stress measurement system. The highfrequency SiN<sub>x</sub> film has been determined to induce a tensile strain of 347 MPa while the low-frequency SiN<sub>x</sub> film has been determined to induce a compressive film of -797 MPa. The high-frequency and low-frequency sourced SiNx films are then employed as masks for IID aperture formation. As shown in Fig. 3, the IID apertures resulted in distinctly different geometries as a result of the contrasting strains induced in the different SiNx diffusion masks.

Through periodically time-alternating the high-frequency and low-frequency source times during the deposition of

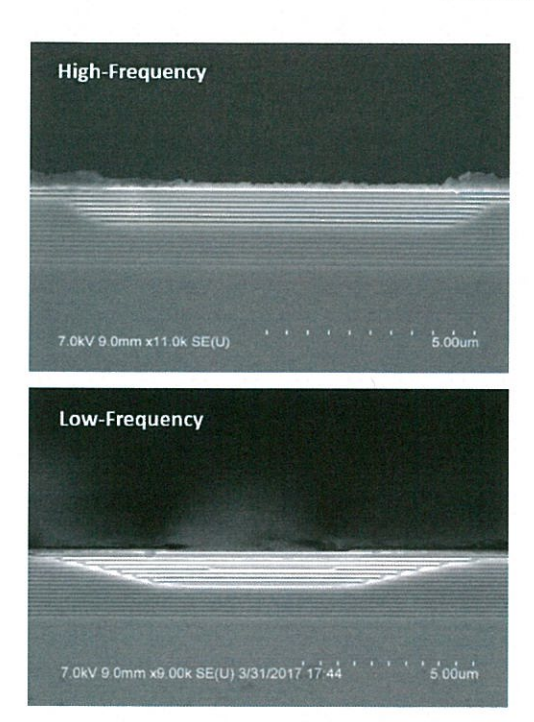


Fig. 3. SEM images of IID apertures in DBR strained by a high-frequency sourced (top) and low-frequency sourced (bottom) PECVD grown  $SiN_X$  diffusion mask.

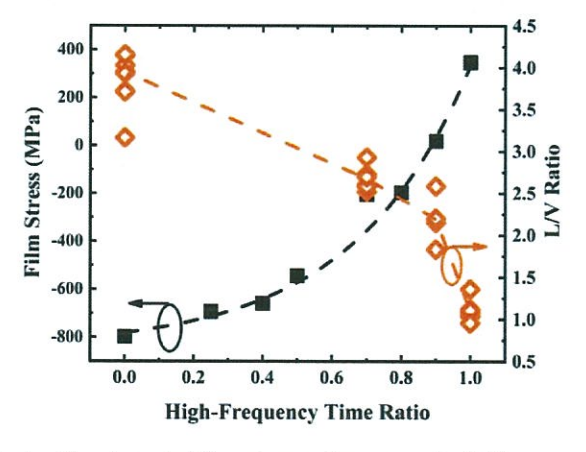


Fig. 4. The change in IID aperture profile as a result of different strain induced by the diffusion mask.

mixed-frequency  $SiN_x$  films, the strain of the diffusion mask can be engineered to any value between the two limits. For mixed-frequency  $SiN_x$  films, the deposition begins with high-frequency  $SiN_x$  deposition followed by a low-frequency  $SiN_x$  such that the total deposition time is 20 seconds. This process is then periodically repeated for a total target deposition thickness of 50 nm. The mixed-frequency  $SiN_x$  films are then defined by the ratio of high-frequency time in each 20 second period. As shown in Fig. 4, by increasing high-frequency deposition time ratio in the mixed-frequency nitride film, the induced strain of the film increases with an exponential-like behavior. The 0.70 and 0.90 high-frequency sourced time ratio mixed-frequency films are then employed for IID aperture formation.

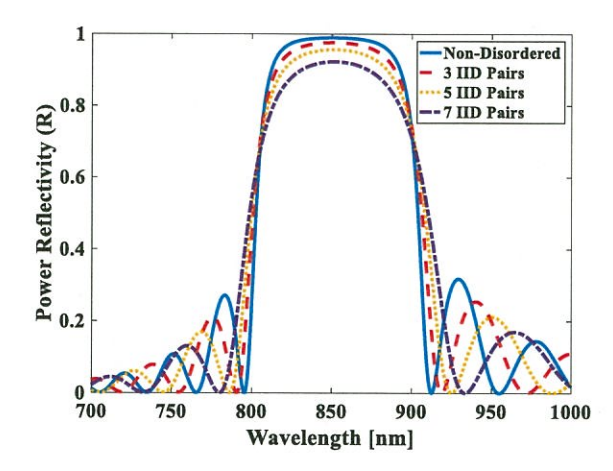


Fig. 5. Effect of disordering on the upper DBR power reflectivity for a given number of IID pairs.

In order to quantify the various IID aperture profiles, the lateral-to-vertical (L/V) ratios of their diffusion fronts are measured. In Fig. 4, it is shown that the L/V ratios decrease with an exponential-like behavior that is inversely related to the strain induced by the diffusion masks. This demonstrates a controllable method of tailoring the IID aperture profile by modifying the strain induced by the SiN<sub>x</sub> diffusion mask that is compatible with wafer-scale processing.

# VI. MODE BEHAVIOR ANALYSIS

In order to perform modeling and an analysis on the modal behavior of VCSELs with various sized IID apertures, numerical calculations of the net power reflectivity of the disordered DBR and the evolution of the guided modes are presented. The one-dimensional (1D) transfermatrix method (TMM) is employed to calculate the power reflectivity of the upper DBR for a given number of disordered pairs. Al<sub>0.15</sub>Ga<sub>0.85</sub>As-Al<sub>0.90</sub>Ga<sub>0.1</sub>As based DBR with 20 pairs is modeled with a GaAs cap. The disordered region is assumed to be completely disordered resulting in a homogenous bulk Al<sub>x</sub>Ga<sub>1-x</sub>As layer with an averaged aluminum composition [14], [15]. As a result, the disordered region is represented by an Al<sub>0.525</sub>Ga<sub>0.475</sub>As composition. As reported in literature, the index of refraction for AlAs and GaAs are found to be 2.9858 [24] and 3.6480 [25] for 850 nm at 300 K. The index refraction of the Al<sub>x</sub>Ga<sub>1-x</sub>As layers were calculated using Vegard's Law in ternary III-V alloys which resulted in the following indices of refraction:

By employing the TMM, the resulting power reflectivity for a given number of disordered pairs is numerically calculated. Using the backward propagation matrix approach, the net power reflectivity of multiple planar interfaces alternating between Al<sub>0.15</sub>Ga<sub>0.85</sub>As/Al<sub>0.90</sub>Ga<sub>0.1</sub>As layers can be calculated [26]. In the non-disordered case, the modeled epitaxial layer consists of 20 Al<sub>0.15</sub>Ga<sub>0.85</sub>As/Al<sub>0.90</sub>Ga<sub>0.1</sub>As pairs covered by a GaAs cap layer. For the disordering cases, the top Al<sub>x</sub>Ga<sub>1-x</sub>As pairs are assumed to be completely disordered therefore being represented by Al<sub>0.525</sub>Ga<sub>0.475</sub>As layers in this calculation. Shown in Fig. 5, It is apparent that the disordering causes both the magnitude and bandwidth of the mirror

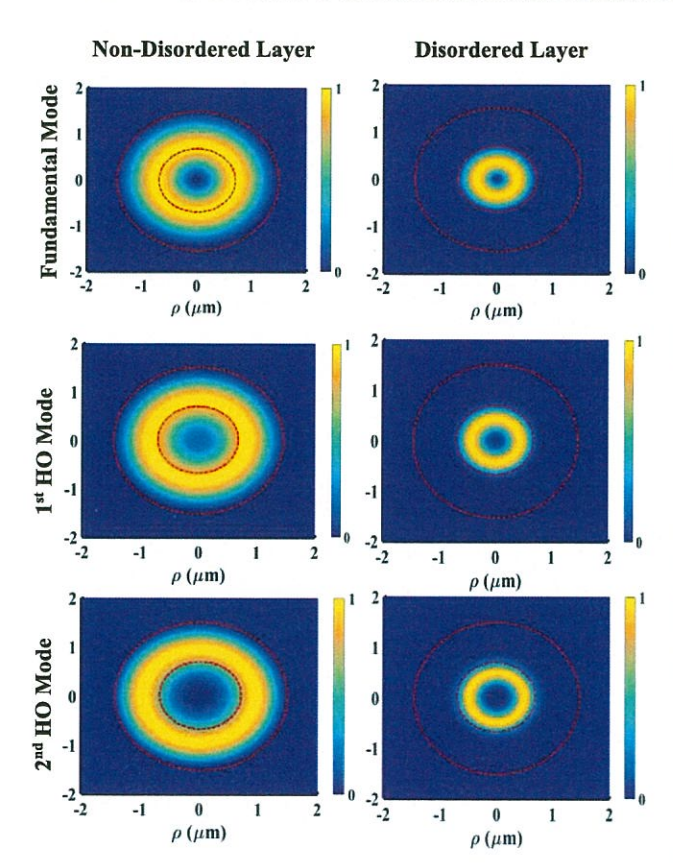


Fig. 6. Normalized power distribution of the first three propagating modes in a non-disordered layer (left column) and disordered layer (right column). The outer dotted red line indicates the boundary of the 3.0  $\mu$ m oxide aperture and the inner dotted red line indicates the boundary of the 1.3  $\mu$ m IID aperture. HO denotes Higher Order mode.

 $TABLE \ I \\ Index \ of \ Refraction \ for \ Al_xGa_{1-x}As \ Used \ in \ TMM \\$ 

$Al_{0.15}Ga_{0.85}As$	Al <sub>0.525</sub> Ga <sub>0.475</sub> As	Al <sub>0.90</sub> Ga <sub>0.10</sub> As
3.54996	3.30486	3.05976

power reflectivity to decrease and the effect is greater for larger degrees of disordering. As a result, when higher order modes overlap with the disordering regions, they experience an increase in threshold modal gain thereby suppressing lasing.

Mode suppression is optimized when only the higher order modes are affected by disordering while the fundamental-mode is unaffected. A numerical calculation that exhibits the spatial distribution of the modes as it propagates through the disordered upper DBR is therefore necessary to optimize the IID aperture size for any application. The optimal IID aperture size of 1.3  $\mu m$  for an oxide aperture sized device of 3.0  $\mu m$  yielded maximum single-fundamental-mode power [16], [17]. The power distribution of the first three propagating modes are calculated for a VCSEL with a 1.3  $\mu m$  IID aperture and a 3.0  $\mu m$  oxide aperture.

Utilizing the TMM, the electric and magnetic fields can be calculated in each DBR layer. The model assumes an infinitely long cylinder with multiple claddings that extends infinitely in the longitudinal direction. The core represents the

TABLE II ENERGY FLUX OVERLAP AT THE INTERFACE BETWEEN NON-DISORDERED AND DISORDERED DBR

Fundamental	1st HO Mode	2 <sup>nd</sup> HO Mode
0.6769	0.6407	0.4578

DBR while the claddings represent the disordered and oxide aperture regions. The spatial energy flux, which is represented by the Poynting vector, can then be calculated from the set of optical eigenmodes and their corresponding mode profile. The Poynting vector follows the power orthogonality relation:

$$\int_{S} \left( \mathbf{E}_{is} \times \mathbf{H}_{js}^{*} \right) \cdot \hat{z} dS = 0, \quad \text{if} \quad i \neq j$$

where i and j represent the index of the mode given in the longitudinal direction. A rigorous analysis of the power transmission between propagating optical modes through each layer requires the calculation of mode matching. However, mode matching is mathematically quantified by the overlap integral between each mode in order to determine the coupling efficiency of the modes. Therefore, the spatial overlap integral between the energy flux at the interface of the disordered and non-disordered region provides a general physical picture of the transition of modes when the higher order modes are incident on the IID aperture.

In Fig. 6, the numerical calculation of the normalized power distribution for the first three propagating modes in a non-disordered DBR layer and a disordered DBR layer is shown. The oxide (outer rings) and IID apertures (inner rings) are outlined with dotted red circles to denote where the disordering region affects the mode. It is shown that the power distribution of the fundamental mode primarily resides near the center of the device for both non-disordered and disordered regions. Using the calculated power distributions, the overlap integral between a mode in the non-disordered region and the same mode in the disordered region is calculated. This will provide a numerical analysis of the power transmittivity between the layer discontinuity caused by disordering.

Shown in Table II, the fundamental mode and the 1st higher order mode show the largest energy flux overlap at the interface between the non-disordered and disordered layer. Further higher-order modes begin to decrease in energy flux overlap at the discontinuous interface which suggests that these higher order modes are scattered at the interface. The comparable energy flux overlap of the fundamental mode and the 1st higher order mode suggests that the 1st higher order mode is quite likely to transmit similarly like the fundamental mode. This is consistent with the experimental work done in [16] and [17], where the first higher order mode began to appear at larger driving currents. It must be noted that the energy flux overlap calculated is based on normalized power distributions. The fundamental mode exhibits an energy flux magnitude that is approximately three-orders larger in magnitude than the 1st higher order mode.

## VII. CONCLUSION

In summary, impurity-induced disordering and its application to mode control in vertical-cavity surface-emitting

lasers is discussed. The limited control of IID apertures with standard diffusion masks motivates the development of a wafer-scale compatible method of modifying the shape of the diffusion front. Through altering the strain induced by the diffusion mask, the geometric shape of the IID aperture can be extensively controlled. Numerical calculations of the mode behavior as a result of impurity-induced disordering are also presented. These results can be used to implement future IID aperture designs for improved and more complex high-power single-mode performance.

#### ACKNOWLEDGMENT

The authors would like to thank the CS MANTECH technical program committee for their invitation of this special issue.

### REFERENCES

- H. Moench et al., "VCSEL-based sensors for distance and velocity," in Proc. Vertical Cavity Surface Emitting Lasers XX, vol. 9766. San Francisco, CA, USA, 2016, Art. no. 97660A. [Online]. Available: https://doi.org/10.1117/12.2209320
- [2] I. Melngailis, "Longitudinal injection-plasma laser of InSb," Appl. Phys. Lett., vol. 6, no. 3, pp. 59–60, 1965. [Online]. Available: https://doi.org/10.1063/1.1754164
- [3] H. Soda, K.-I. Iga, C. Kitahara, and Y. Suematsu, "GaInAsP/InP surface emitting injection lasers," *Jpn. J. Appl. Phys.*, vol. 18, no. 12, p. 2329, 1979. [Online]. Available: https://doi.org/10.1143/JJAP.18.2329
- [4] D. R. Scifres and R. D. Burnham, "Distributed feedback diode laser," U.S. Patent 3 983 509, Sep. 28, 1996.
- [5] J. M. Dallesasse, N. Holonyak, Jr., A. R. Sugg, T. A. Richard, and N. El-Zein, "Hydrolyzation oxidation of Al<sub>x</sub>Ga<sub>1-x</sub>As-AlAs-GaAs quantum well heterostructures and superlattices," *Appl. Phys. Lett.*, vol. 57, no. 26, pp. 2844–2846, 1990. [Online]. Available: https://doi.org/10.1063/1.103759
- [6] J. M. Dallesasse and D. G. Deppe, "III–V oxidation: Discoveries and applications in vertical-cavity surface-emitting lasers," *Proc. IEEE*, vol. 101, no. 10, pp. 2234–2242, Oct. 2013, doi: 10.1109/JPROC.2013.2274931.
- [7] D. L. Huffaker, D. G. Deppe, K. Kumar, and T. J. Rogers, "Native-oxide defined ring contact for low threshold vertical-cavity lasers," *Appl. Phys. Lett.*, vol. 65, no. 1, pp. 97–99, 1994. [Online]. Available: https://doi.org/10.1063/1.113087
- [8] C. Jung et al., "4.8 mW singlemode oxide confined top-surface emitting vertical-cavity laser diodes," Electron. Lett., vol. 33, no. 21, pp. 1790–1791, Oct. 1997, doi: 10.1049/el:19971207.
- [9] H. Martinsson et al., "Transverse mode selection in large-area oxide-confined vertical-cavity surface-emitting lasers using a shallow surface relief," *IEEE Photon. Technol. Lett.*, vol. 11, no. 12, pp. 1536–1538, Dec. 1999, doi: 10.1109/68.806837.
- [10] E. Soderberg et al., "Suppression of higher order transverse and oxide modes in 1.3-μm InGaAs VCSELs by an inverted surface relief," *IEEE Photon. Technol. Lett.*, vol. 19, no. 5, pp. 327–329, Mar. 1, 2007, doi: 10.1109/LPT.2007.891631.
- [11] D.-S. Song, S.-H. Kim, H.-G. Park, C.-K. Kim, and Y.-H. Lee, "Single-fundamental-mode photonic-crystal vertical-cavity surface-emitting lasers," *Appl. Phys. Lett.* vol. 80, no. 21, pp. 3901–3903, 2002. [Online]. Available: https://doi.org/10.1063/1.1481984
- [12] M. Gêbski et al., "Transverse mode control in high-contrast grating VCSELs," Opt. Express vol. 22, no. 17, pp. 20954–20963, 2014. [Online]. Available: https://doi.org/10.1364/OE.22.020954
- [13] D. Zhou and L. J. Mawst, "High-power single-mode antiresonant reflecting optical waveguide-type vertical-cavity surface-emitting lasers," *IEEE J. Quantum Electron.*, vol. 38, no. 12, pp. 1599–1606, Dec. 2002, doi: 10.1109/JQE.2002.805107.
- [14] W. D. Laidig et al., "Disorder of an AlAs-GaAs superlattice by impurity diffusion," Appl. Phys. Lett., vol. 38, no. 10, pp. 776–778, 1981. [Online]. Available: https://doi.org/10.1063/1.92159

- [15] D. G. Deppe and N. Holonyak, Jr., "Atom diffusion and impurity-induced layer disordering in quantum well III-V semiconductor heterostructures," J. Appl. Phys., vol. 64, no. 12, pp. R93–R113, 1988. [Online]. Available: https://doi.org/10.1063/1.341981
- [16] T. O'Brien, Jr., B. Kesler, S. A. Mulla, and J. M. Dallesasse, "Mode behavior of VCSELs with impurity-induced disordering," *IEEE Photon. Technol. Lett.*, vol. 29, no. 14, pp. 1179–1182, Jul. 15, 2017, doi: 10.1109/LPT.2017.2701647.
- [17] P. Su, T. O'Brien, Jr., F.-C. Hsiao, and J. M. Dallesasse, "Controlling impurity-induced disordering via mask strain for high-performance vertical-cavity surface-emitting lasers," presented at the CS MANTECH, Austin, TX, USA, May 2018.
- [18] J.-W. Shi et al., "Minimization of damping in the electrooptic frequency response of high-speed Zn-diffusion single-mode verticalcavity surface-emitting lasers," *IEEE Photon. Technol. Lett.*, vol. 19, no. 24, pp. 2057–2059, Dec. 15, 2007, doi: 10.1109/LPT.2007.910087.
- [19] J.-W. Shi, J.-C. Yan, J.-M. Wun, J. Chen, and Y.-J. Yang, "Oxide-relief and Zn-diffusion 850-nm vertical-cavity surface-emitting lasers with extremely low energy-to-data-rate ratios for 40 Gbit/s operations," *IEEE J. Sel. Topics Quantum Electron.*, vol. 19, no. 2, Mar./Apr. 2013, Art. no. 7900208. doi: 10.1109/JSTQE.2012.2210863.
- [20] J.-W. Shi et al., "High-power and high-speed Zn-diffusion single fundamental-mode vertical-cavity surface-emitting lasers at 850-nm wavelength," *IEEE Photon. Technol. Lett.*, vol. 20, no. 13, pp. 1121–1123, Jul. 1, 2008, doi: 10.1109/LPT.2008.924645.
  [21] P. M. Asbeck et al., "GaAlAs/GaAs heterojunction bipolar transistors:
- [21] P. M. Asbeck et al., "GaAlAs/GaAs heterojunction bipolar transistors: Issues and prospects for application," *IEEE Trans. Electron Devices*, vol. 36, no. 10, pp. 2032–2042, Oct. 1989, doi: 10.1109/16.40886.
- [22] Y.-R. Yuan, K. Eda, G. A. Vawter, and J. L. Merz, "Open tube diffusion of Zn into AlGaAs and GaAs," J. Appl. Phys., vol. 54, no. 10, pp. 6044–6046, 1983. [Online]. Available: https://doi.org/10.1063/1.331750
- [23] B. Kesler, T. O'Brien, G.-L. Su, and J. M. Dallesasse, "Facilitating single-transverse-mode lasing in VCSELs via patterned dielectric anti-phase filters," *IEEE Photon. Technol. Lett.*, vol. 28, no. 14, pp. 1497–1500, Jul. 15, 2016, doi: 10.1109/LPT.2016.2555294.
- [24] R. E. Fern and A. Onton, "Refractive index of AlAs," J. Appl. Phys., vol. 42, no. 9, pp. 3499–3500, 1971. [Online]. Available: https://doi.org/10.1063/1.1660760
- 25] S. Ozaki and S. Adachi, "Spectroscopic ellipsometry and thermore-flectance of GaAs," J. Appl. Phys., vol. 78, no. 5, pp. 3380–3386, 1995. [Online]. Available: https://doi.org/10.1063/1.359966
- 26] S. L. Chuang, Physics of Photonic Devices, vol. 80. New York, NY, USA: Wiley, 2012.



Patrick Su (M'16) received the B.S. degree in electrical engineering from the University of Illinois at Urbana–Champaign, Urbana, IL, USA, in 2016, where he is currently pursuing the M.S. and Ph.D. degrees.

Since 2017, he has been a Research Assistant with the Micro and Nanotechnology Laboratory, University of Illinois at Urbana—Champaign conducting research in the field of optoelectronics and active photonic devices for photonic integrated circuit and optical sensing applications.

Mr. Su is a member of Eta Kappa Nu Alpha Chapter with the University of Illinois at Urbana-Champaign.



Fu-Chen Hsiao received the B.S. degree in physics from National Taiwan Normal University, Taipei, Taiwan, in 2010 and the M.S. degree in photonics engineering from National Cheng Kung University, Tainan, Taiwan, in 2012. He is currently pursuing the Ph.D. degree in electrical engineering from the University of Illinois at Urbana-Champaign, Urbana, IL, USA.

Since 2015, he has been a Research Assistant with the Micro and Nanotechnology Laboratory, University of Illinois at Urbana-Champaign con-

ducting research in the field of simulation and modeling of photonic device and nanostructures. His research interests include simulation of electronic, optical and transport properties of semiconductors, nanostructures, and photonic device modeling. Thomas O'Brien, Jr. received the B.S. degree in physics from the University of Notre Dame, South Bend, IN, USA, in 2010 and the M.S. degree in electrical and computer engineering and the Ph.D. degree in electrical engineering from the University of Illinois at Urbana–Champaign, Urbana, IL, USA, in 2012 and 2017, respectively. He is currently with Intel Corporation, Hillsboro, OR, USA.



John M. Dallesasse (F'15) received the B.S., M.S., and Ph.D. degrees in electrical engineering from the University of Illinois at Urbana-Champaign in 1985, 1987, and 1991, respectively. He has over 20 years of experience in the Optoelectronics Industry and six years of experience in academia. He has held a wide range of positions in technology development and management. He was the Chief Technology Officer, the Vice President, and the Co-Founder of Skorpios Technologies, Inc., a company involved in the integration of compound semiconductor materi-

als with silicon in a CMOS-compatible process. He is with the Department of Electrical and Computer Engineering, University of Illinois in Urbana—Champaign, where he is researching on electronic-photonic integration, novel coherent emitters for the mid-IR, and modeling of semiconductor devices. He has over 60 publications and presentations, and 42 issued patents. His technical contributions include, with N. Holonyak, Jr., the discovery of III-V Oxidation—an enabling technology for the fabrication of high-speed vertical-cavity surface-emitting lasers. He also serves as an Associate Editor for the IEEE JOURNAL OF QUANTUM ELECTRONICS. He is on the Steering Committee for the IEEE JOURNAL OF LIGHTWAVE TECHNOLOGY, and the Chair of Steering Committee for the IEEE TRANSACTIONS ON SEMICONDUCTOR MANUFACTURING. He is a member of the American Physical Society, Tau Beta Pi, Eta Kappa Nu, and is a fellow of the Optical Society of America.